ELSEVIER

Biochimica et Biophysica Acta 1558 (2002) 95–108

BIOCHIMICA ET BIOPHYSICA ACTA
BBA

www.bba-direct.com

Interactions of the drug amphotericin B with phospholipid membranes containing or not ergosterol: new insight into the role of ergosterol

J. Milhaud [a,*], V. Ponsinet [b], M. Takashi [c], B. Michels [d]

[a] *Laboratoire de Physico-chimie Biomoléculaire et Cellulaire (ESA 7033), Université Pierre et Marie Curie, P.O. Box 138, 75252 Paris Cedex 05, France*

[b] *Laboratoire de Physique de la Matière Condensée (CNRS URA 792), Collège de France, 11 pl. M. Berthelot, Paris Cedex 05, France*

[c] *Laboratoire de Biocatalyse, FRE 2230, Université de Nantes et CNRS, 2 rue de la Houssinière, 44322 Nantes Cedex 3, France*

[d] *Laboratoire de Dynamique des Fluides Complexes (UA CNRS 851), Université Louis Pasteur, 67070 Strasbourg Cedex, France*

Received 12 July 2001; received in revised form 13 September 2001; accepted 13 September 2001

Abstract

Amphotericin B (AmB) is an amphipathic polyene antibiotic which permeabilizes ergosterol-containing membranes, supposedly by formation of pores. In water, AmB forms chiral aggregates, modelled as stacks of planar dimers in which the joined polyene chains in each dimer turn round, from one dimer to the following in these stacks, by forming a helical array. Studies of the binding of AmB with L-dipalmitoylphosphatidylcholine (L-DPPC) and L-dilauroylphosphatidylcholine (L-DLPC) bilayers disclose the main following results. (1) An inversion of the helicity of the L-DPPC-bound AmB aggregates, when the L-DPPC bilayers are in the gel phase, is inferred from the evolution of the circular dichroism spectra of AmB+L-DPPC mixtures. (2) An AmB-induced gel-to-subgel transformation of L-DPPC bilayers, in the previous mixtures, is revealed by a differential scanning calorimetry study. (3) The role played by ergosterol in the location of phospholipid-bound AmB aggregates with respect to a phospholipid bilayer is directly demonstrated from atomic force microscopy observations of mica-supported AmB+L-DLPC mixtures, in the presence or absence of ergosterol. While in the absence of ergosterol AmB aggregates remained at the surface of the bilayer, in the presence of ergosterol they appeared embedded within this bilayer and became hollow-centered. As such an embedding in the hydrophobic core of a bilayer requires a rearrangement of the aggregates with respect to their architecture in water, this rearrangement is held responsible for the hollowing of aggregates. The hollow-centered sublayer-embedded AmB aggregates are thought to be the precursors of the formation of AmB pores.

Keywords: Helical amphotericin B aggregate; Amphotericin B pore; Ergosterol-containing bilayer; Chirality; Differential scanning calorimetry; Atomic force microscopy

1. Introduction

Amphotericin B (AmB, Fig. 1_1) is a chiral polyene antibiotic which permeabilizes ergosterol-containing membranes, like membranes of fungal cells, and thus has an antifungal action. It is generally accepted ([1] and references herein, [2] and references herein, [3]) that this permeabilization results from the for-

Abbreviations: AmB, amphotericin B; L-DPPC, L-dipalmitoylphosphatidylcholine; L-DLPC, L-dilauroylphosphatidylcholine; AFM, atomic force microscopy; CD, circular dichroism; DSC, differential scanning calorimetry; DMF, dimethylformamide; NBD-PE, *N*-(7-nitrobenz-2-oxa-1,3-diazol-4-yl)-1,2-dihexadecanoyl-*sn*-glycero-3-phosphoethanolamine, triethylammonium salt

* Corresponding author. Fax: +33-1-44277560.

E-mail address: milhaud@lpbc.jussieu.fr (J. Milhaud).

0005-2736/02/$ – see front matter
PII: S0005-2736(01)00416-3

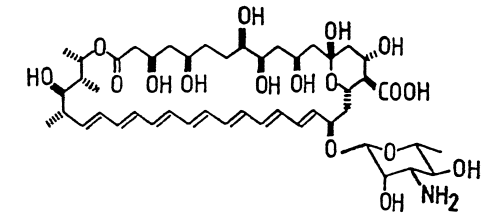

1

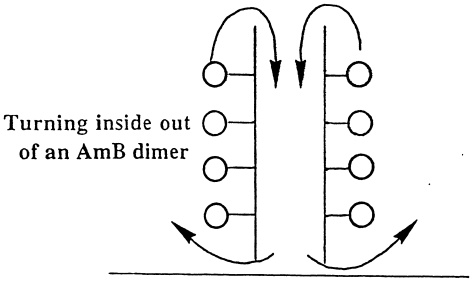

2

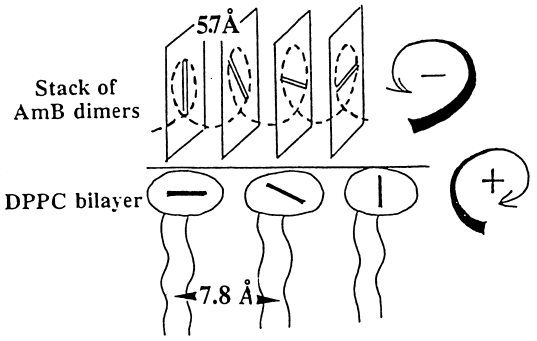

3

Fig. 1. (1) Developed formula of amphotericin B. (2) Sketch of a turning inside out of an AmB dimer oriented perpendicularly to the interface of the membrane (the hydroxyl groups and the polyene chain of AmB molecules are schematized by circles and solid straight lines, respectively). (3) Sketch of the chiral assemblies of L-DPPC and AmB molecules at the membrane–water interface. One AmB oligomer is schematized by parallel planes spaced by 5.7 Å (as planar AmB dimers in the double helix model [21]). The joined polyene chains of each dimer were schematized by two dashes turning counterclockwise. DPPC molecules are schematized by two undulating lines (the fatty chains) attached to one ellipse (the polar head) in which the P^{-}-N^{+} dipole is schematized by a dash turning clockwise.

mation of pores. However, such pores have never yet been visualized and their existence is strongly questioned by recent results [4,5].

On the other hand, in the absence of sterol, AmB molecules, when they bind to L-dilauroylphosphatidylcholine (L-DLPC) bilayers, remain at the exterior of these membranes [6]. Hence, two relevant questions emerge: (i) what is the role played by the membranous ergosterol?; (ii) what type of bond bridges AmB molecules and sterol-free phospholipid membranes at the membrane–water interface? Our investigations, aimed at answering these questions, have involved three methods and two types of mixtures. They disclose original phenomena occurring at the membrane–water interfaces. Moreover, atomic force microscopy (AFM) observations directly demonstrate what is the role of ergosterol, making it possible to throw new light on the mechanism of the formation of AmB pores.

2. Materials and methods

2.1. Materials

L-DLPC and L-dipalmitoylphosphatidylcholine (L-DPPC) were purchased from Sigma (St. Louis, MO, USA) and used without further purification. Their concentrations were determined by Stewart's method [7]. Ergosterol was recrystallized two times. AmB was a generous gift of Bristol-Myers-Squibb (La Défense, Paris, France). It was stored at 6°C, in the presence of dry argon, to prevent any hydration. Its concentration was deduced from the absorbance in methanol ($\varepsilon_{409} = 1.56 \times 10^5$ M^{-1} cm^{-1} [6]). *N*-(7-Nitrobenz-2-oxa-1,3-diazol-4-yl)-1,2-dihexadecanoyl-*sn*-glycero-3-phosphoethanolamine, triethylammonium salt (NBD-PE) was purchased from Molecular Probes (Interchim, Paris, France).

2.2. AmB+L-DPPC mixtures (mixtures I)

The mixtures I were prepared by adding small volumes of a concentrated vesicle suspension to a large volume of an AmB buffered solution (no change of the AmB concentration). L-DPPC vesicles were prepared by evaporating the desired amount of a chloroformic L-DPPC solution in vacuum, for several hours. The resulting dried film was then dispersed in a phosphate buffer, at a temperature 10°C higher than the gel-to-fluid transition, and subjected to a probe sonication, until a complete clearing of the

dispersion. In order to narrow the size distribution of vesicles, the dispersion was filtered with an extruder, through 0.1 μm polycarbonate filters, and the final size distribution checked by QELS with a Coulter N4 Plus. The polydispersity index of this distribution was equal to 0.3. The mean diameter of vesicles was 90 nm. The AmB content of the mixtures is given by the antibiotic-to-phospholipid molar ratio, R_A.

Given the long duration of the L-DPPC+AmB association reaction, the preservation of AmB aqueous solutions was taken care of. In some mixtures, to make sure that the results were not biased by any oxidation of AmB, argon was bubbled through the samples, to eliminate oxygen. As the corresponding results were the same as those obtained with aerated samples, screened from UV irradiation, we pursued our measurements without any bubbling of argon. In the dark, an AmB aqueous solution can be stored safely for 25 days.

2.3. Absorption and circular dichroism (CD) measurements

UV absorption spectra were obtained with a Cary 1E spectrophotometer. CD spectra were recorded with a Jobin Yvon Mark IV dichrograph. The dichrograph and the spectrophotometer were equipped with thermostated cuvette holders. $\Delta\varepsilon$ is the differential extinction coefficient. Spectra were corrected for the light scattering by vesicles, by subtracting from the spectra of AmB-containing mixtures the spectra obtained in the same cuvette by replacing AmB by the buffer. A smoothing of the spectra, owing to the Kaleidagraph software, was only used when noted in the figure legends.

2.4. Calorimetric measurements

High-sensitivity calorimetric measurements were performed on a DASM-4 microcalorimeter [8], interfaced to a Bull Micral computer. To determine the enthalpy corresponding to an endotherm, a straight line was traced between its onset and its completion temperatures and the corresponding surface calculated with the software provided by Microcal.

2.5. Mica-supported AmB+L-DLPC mixtures (mixtures II)

The mixtures II were prepared by coevaporating the desired volumes of an AmB methanolic solution and a phospholipid chloroformic solution and, if desired, an ergosterol chloroformic solution. The chosen aliquots corresponded, without and with ergosterol, to the composition: 1.9×10^{-4} M L-DLPC/4×10^{-7} M AmB. This film was dispersed in water and lyophilized. The resultant powder was dispersed in a 10^{-2} M HEPES, 0.15 M NaCl (pH 7) buffer and subjected to probe sonication. The resultant vesicles were centrifuged at 10 000 rpm for 15 min to eliminate the titanium particles. The ergosterol content of the mixtures is given by the ergosterol-to-phospholipid molar ratio, R_E.

Mica-supported preparations were performed in a homemade flow cell using the vesicle fusion method [9]. In this cell, a circulation of mixtures II, above a freshly cleaved mica wafer, was carried out with a peristaltic pump. Optimal conditions to obtain a single bilayer mean coverage (referring to the known area per L-DPPC polar head, in the fluid state, of 64 $Å^2$ [11]) were derived from the study of the fluorescence of a lipid film formed on mica by fusion of vesicles of 10% NBD-PE-labelled L-DLPC [10]. They were: circulation of mixtures with a flow rate of 15 ml h^{-1} for 3 h, a 14 h long incubation after stopping the circulation and a rinsing with a 10^{-2} M HEPES buffer with a flow rate of 75 ml h^{-1} for 20 min.

The mica-supported preparation was then transferred, under water immersion, to a homemade fluid cell suitable for AFM imaging. Let us stress that the preparation was never in contact with air in order to keep it in its native state.

2.6. AFM imaging

An Autoprobe CP microscope (Park Scientific Instruments) and a 100 μm scanner were used. Two imaging modes were used. Contact mode imaging was performed, under water immersion, with a silicon nitride cantilever of nominal spring constant 0.1 N/m, using nominal applied forces between 0.5 and 9 nN. Intermittent contact mode imaging [12] in air,

after removal of water, was also used with a silicon cantilever of nominal spring constant 6 N/m and with a working oscillation amplitude of the order 10 nm.

Both topography and error signal images [13] were recorded, consisting of 256×256 pixels, with size ranging from 1 to 40 μm and scanning frequencies ranging from 0.2 to 20 Hz.

Let us stress that the main precaution to be taken when imaging soft and weakly immobilized objects such as ours, in contact mode, is to prevent the penetration of the tip into the sample. For that purpose, first, the applied force should be chosen as small as possible and, second, the scanning rate should be large enough so that the tip surfs on the surface [14]. The first reduces the stability of the contact and may produce instabilities in the images. The second reduces the sampling time and, thus, the resolution. The optimal conditions to obtain reproducible images in successive scans, without displacement of material, were found to be a nominal applied force lower than 1 nN and a scanning rate higher than 6 μm s^{-1}. On some of the studied preparations, we deliberately used higher forces and scanning rates in order to scratch the soft sample surface on a limited area. The depth of the scratched hole was measured by carrying out a larger scan at the same place, with imaging conditions (cf. above).

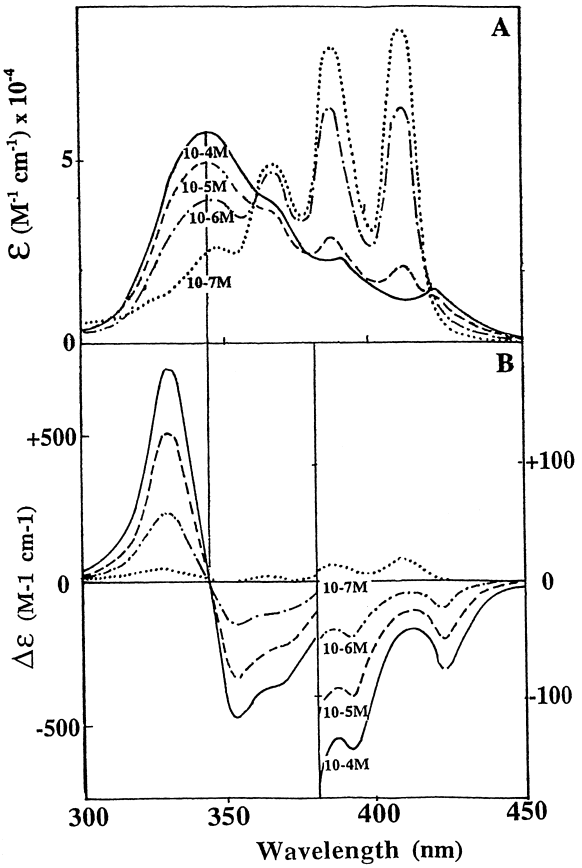

Fig. 2. Absorption (A) and CD (B) spectra of AmB buffered solutions as a function of the concentration (buffer: Tris–HCl 50 mM, pH 7.5) (redrawn from [15]).

3. Results

3.1. Properties of pure AmB aqueous solutions

AmB molecules are poorly soluble in water and, owing to their amphipathicity, form aggregates beyond a concentration of around 2×10^{-7} M^{-1} in water [15]. Let us note that this concentration is not a critical micellar concentration and AmB aggregates are expected to be polydispersed in size. Within these aggregates, the chromophores of the neighboring monomers (the polyene chains) interact. The consequences of this coupling ('exciton splitting' [16]) are, as shown in Fig. 2 [15]: (i) in absorption, a blue shift of the absorption region (replacement of the vibrational progression by a broad band centered at 340 nm); (ii) in CD, the appearance of a bisignate doublet (long wavelength negative, short wavelength positive) centered at the maximum of the broad absorption band.

3.2. AFM observation of sterol-free mixtures II ($R_A = 2\times10^{-3}$), at room temperature

The surface of the mica-supported sterol-free pure L-DLPC samples (no AmB) appeared plain. Scratching it out with the tip, down the mica, revealed the presence of a layer with a thickness near that known for a fluid L-DLPC bilayer (33 Å [17], Fig. 3). By contrast, in the presence of AmB, this surface appeared entirely covered by objects polydispersed in size (images 1 and 2 in Fig. 4, height profile C). These objects were not displaced during the scanning of the surface with the tip if the nominal applied force was lower than 1 nN (contact mode imaging, cf. Section 2). We infer that they are loosely bound to the sublayer. In this regard, let us recall that the

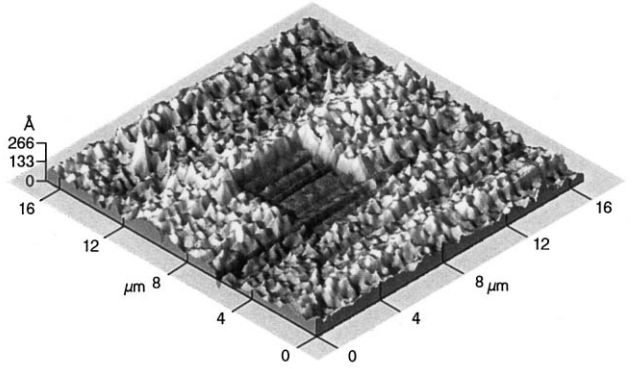

Fig. 3. Surface of a mica-supported pure L-DLPC membrane, in the fluid state, viewed by a topography image, obtained in contact mode, in water, and displayed with a 3D representation. The dug square results from a scratching out by the tip and reveals that the thickness of the membrane is equal to 34 Å.

preparation of the sample implies a complete immersion in water: the persistence of such objects, despite this immersion, demonstrates that they are bound to the sublayer.

To identify these objects, we introduced in the fluid cell a small volume (10% v/v) of a specific solvent of AmB in which phospholipids do not dissolve, dimethylformamide (DMF). Within a delay of 40 min all the objects disappeared (compare images 2 and 3 and height profiles A and C in Fig. 4). We have inferred that these sublayer-bound objects are AmB aggregates. The preserved integrity of the L-DLPC sublayer was demonstrated, as previously, by scratching out with the tip (image 3 in Fig. 4, height profile A).

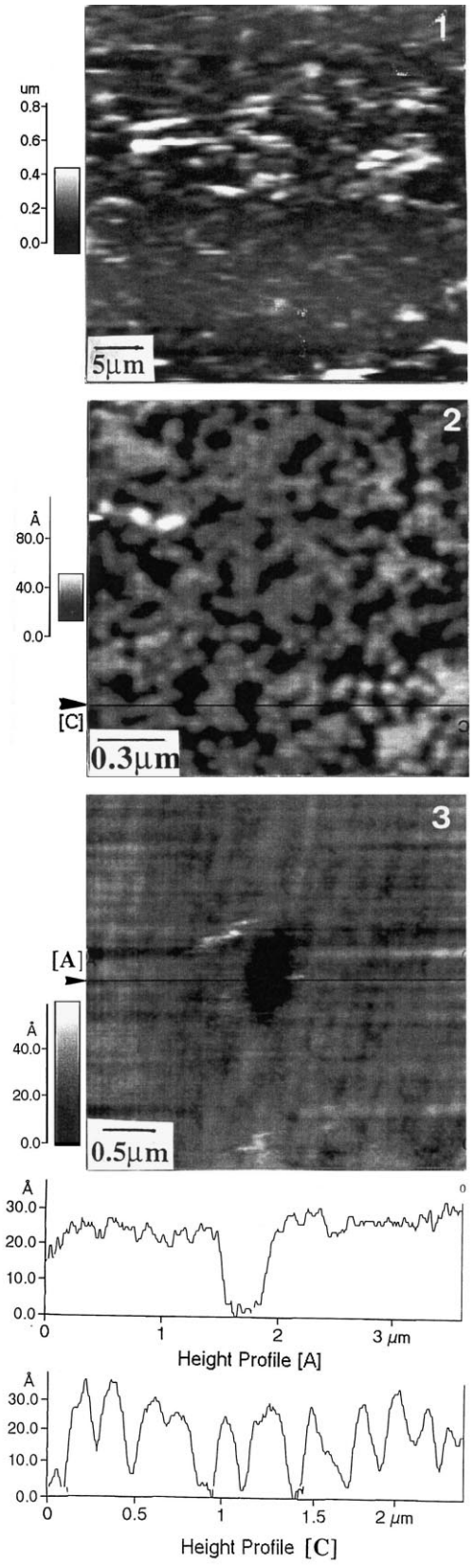

Fig. 4. Surface of a mica-supported sterol-free mixture II with [AmB]/[L-DLPC] = 2×10^{-3} (cf. Section 2), viewed by topography images obtained in contact mode, in water. While at a large scale (image 1, 40×40 μm) some regions appeared free from object, at a small scale (image 2, 2×2 μm) much smaller objects (height profile C) completely stud the surface. By addition of 10% v/v of DMF in the fluid cell, all these objects disappeared after 40 min (image 3, compare the ups and downs of the surface in the height profiles A and C). The preserved integrity of the L-DLPC sublayer is demonstrated by scratching out with the tip (revealing its thickness as the depth of a valley on the height profile A). The streaks observed in image 1 result from instabilities in the tip contact (cf. Section 2). The gray bars are representations of the differential heights.

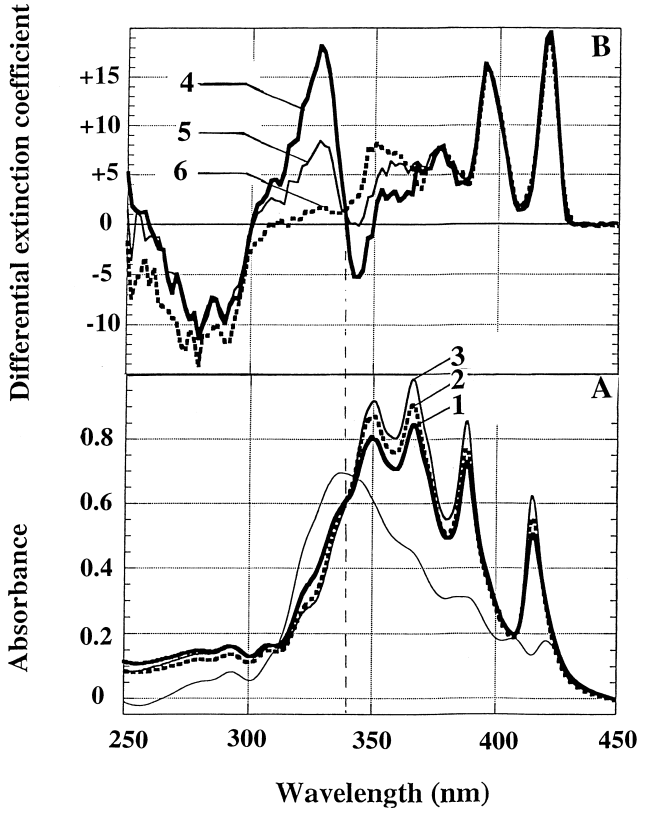

Fig. 5. Absorption (A) and CD (B) spectra of a mixture I (cf. Section 2) with [L-DPPC]/[AmB] = 50 and an AmB concentration of 40 μM, as a function of an incubation at 6°C, for Δt hours (1: $\Delta t = 1$ h; 2: $\Delta t = 4$ h; 3: $\Delta t = 10$ h; 4: $\Delta t = 24$ h; 5: $\Delta t = 48$ h; 6: $\Delta t = 380$ h). The absorption band of the pure AmB solution (thin line) is shown for comparison. The occurrence of an isosbestic and an isodichroic point at the wavelength of the maximum of the absorption band of the pure AmB solution (340 ± 2 nm) is marked by a vertical dashed line. A slight smoothing of CD spectra, owing to the Kaleidagraph software, was carried out to make the superposition of the spectra clearer.

3.3. CD and differential scanning calorimetry (DSC) studies of mixtures I at 6°C

We expected that, in mixtures of AmB+L-DPPC small unilamellar vesicles (SUV; mixtures I), as observed with mixtures II, AmB aggregates would remain at the interface of the bilayers with water. The two following investigations have made it possible to disclose some transformations of AmB and phospholipid polymolecular assemblies which argue for such an interfacial location of AmB aggregates.

3.3.1. Changes of the absorption and CD spectra

Absorption and CD spectra of mixtures I with $8 \leq 1/R_A \leq 100$ (AmB concentration 40 μM) were followed at two temperatures. At 45°C (L-DPPC bilayers in the fluid phase) CD spectra evolve in a few days by exhibiting only a blue shift and a weakening in amplitude of the doublet (not shown). In contrast, at 6°C (L-DPPC bilayers in the gel phase), these spectra keep on evolving slowly for a very long time (up to 20 days) by exhibiting an inversion of the sign of the doublet (Figs. 5B and 6). More precisely, the changes of these spectra implied two steps. First, the CD doublet decreased in amplitude by a factor of 30 (not shown), three positive bands replaced the negative bands of pure AmB and two negative bands appeared (Fig. 5B). Second, over a period longer than 20 days, only the central part of the spectra slowly changed with an inversion of the sign of the doublet, through an isodichroic point located at the maximum wavelength of the broad absorption band of AmB aggregates (340 ± 2 nm, Fig. 6). On absorption spectra (Fig. 5A), this broad band completely disappeared in a few hours, for the benefit of a vibrational progression red-shifted with respect to that of pure AmB. This evolution occurred through an isosbestic point located at the same wavelength as the isodichroic point of CD spectra.

Quantitative measurements of these changes demonstrate that an actual association, with a definite number of saturable binding sites, occurred. The first step of the reaction was followed with mixtures I with $1/R_A < 7.5$ for which the second step of the changes of CD spectra did not occur. From a comparison of the remaining amplitudes of the doublet, at the completion of the reaction, with that of pure AmB, the remaining free AmB concentrations, at each $1/R_A$, were determined. The bound AmB concentrations were deduced by difference. We treated these data by using the following isodesmic model. L-DPPC molecules (approximated as a substrate S) were assumed to hold n identical binding sites with the same apparent association constant, k_{app}, to which the AmB molecules (approximated as a ligand L) bound. The mean number, i, of AmB molecules bound to one L-DPPC molecule, according to this model, is [18,19]:

$$i = \frac{[L_{bound}]}{[S]} = \frac{n \times k_{app}[L_{free}]}{1 + k_{app}[L_{free}]} \quad (1)$$

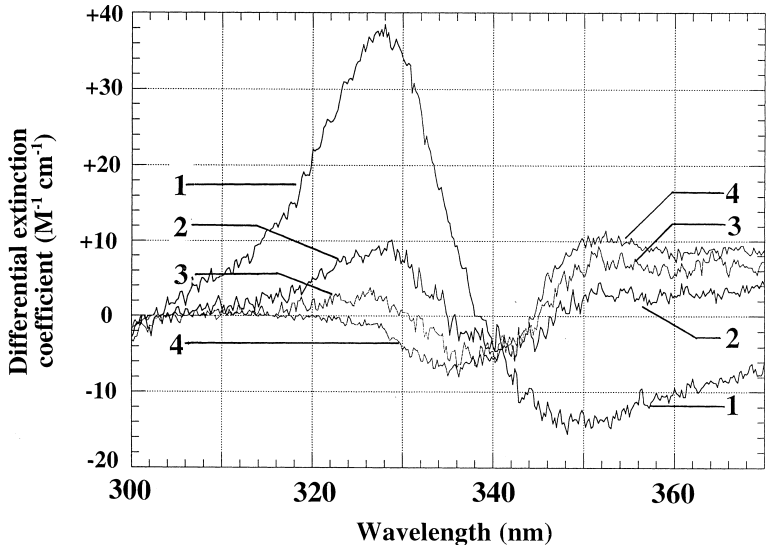

Fig. 6. Central part of the CD spectra of a mixture I (cf. Section 2) with [L-DPPC]/[AmB] = 12 and an AmB concentration of 40 μM, as a function of an incubation at 6°C, for Δt hours (1: $\Delta t = 47$ h; 2: $\Delta t = 171$ h; 3: $\Delta t = 315$ h; 4: $\Delta t = 550$ h).

Eq. 1 can be written as:

$$\frac{[L_{free}] \times [S]}{[L_{bound}]} = \frac{[L_{free}]}{n} + \frac{1}{n \times k_{app}} \quad (2)$$

The left-hand side of Eq. 2 is plotted as a function of L_{free} in Fig. 7. A linear regression of this plot leads to: $k_{app} = 1.8 \times 10^6$ M^{-1} and $n = 1/R_A = 6$.

The second step of the evolution of the CD spectra (the inversion of the doublet, Fig. 6) was followed with mixtures I with $7.5 < 1/R_A < 25$. The final stoichiometry of the association was determined by applying the 'mol ratio method' [19]. We chose, as a parameter characteristic of the association, the amplitude of the inverse dichroic doublet. As shown in Fig. 8, the molar ratio for which this amplitude reached a maximum (the final association stoichiometric ratio) is $[1/R_A]_{final} = 17$.

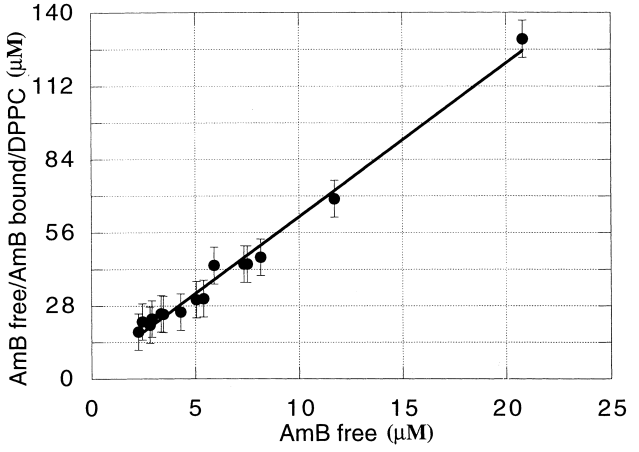

Fig. 7. Linear plot of the isotherm, at 6°C, of the binding of AmB to L-DPPC vesicles. The remaining free AmB concentrations, in each mixture, were calculated from the remaining amplitude of the dichroic doublet at the completion of the reaction (~23 days). The bound AmB concentrations were obtained by difference. The solid straight line corresponds to a linear regression of the experimental points, according to Eq. 2 (see text).

3.3.2. Changes of the DSC thermograms

L-DPPC vesicles from a same batch (3.4 mM

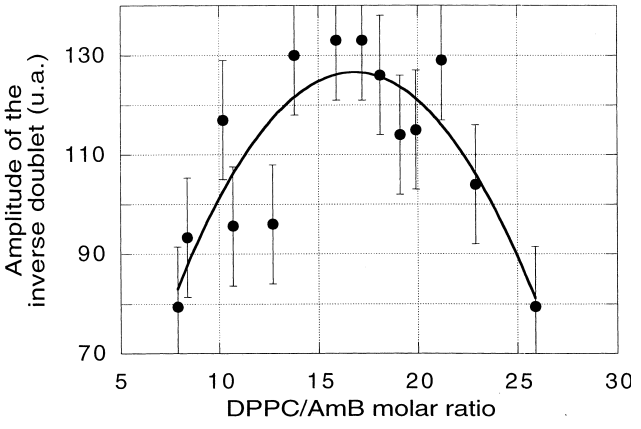

Fig. 8. Amplitudes of the inverse dichroic doublet of the CD spectra of mixtures I (cf. Section 2), with different [L-DPPC]/[AmB] = $1/R_A$ molar ratios (AmB 40 μM), at the completion of the reaction (~23 days), as a function of $1/R_A$.

L-DPPC) mixed or not with AmB ($R_A = 5\times10^{-3}$ and 2.5×10^{-3}) were incubated at 6°C and sampled at different incubation times for DSC measurements. Heating thermograms, between 10 and 50°C, were performed at a heating rate of 0.5°C/min. The pure L-DPPC vesicles exhibited only the endotherm corresponding to the main gel-to-fluid transition, which peaked at 42°C (Fig. 9, traces a and b, enthalpy of 30 kJ/mol in agreement with that of pure L-DPPC large unilamellar vesicles [20]). In contrast, the thermograms of mixtures exhibited the two following additional endotherms (Fig. 9, traces 1–8): (i) a pretransition, at 35.1°C; (ii) a new endotherm appearing only at the first heating scan (not shown). Upon increasing the incubation time at 6°C, the maximum temperature of the latter endotherm shifted from

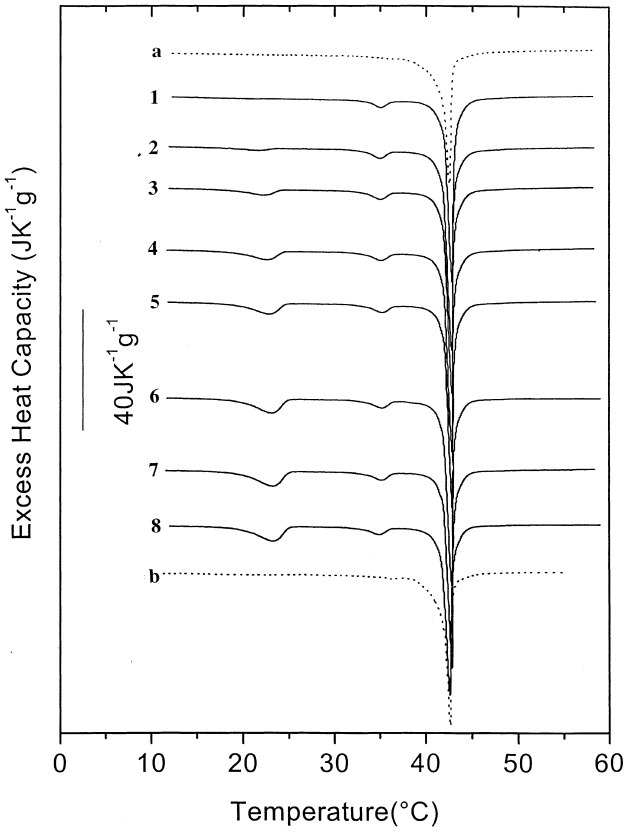

Fig. 9. Heating thermograms of L-DPPC vesicles (3.4 mM L-DPPC) mixed with AmB ([AmB]/[L-DPPC] = 5×10^{-3}, solid lines) or not (dotted lines) as a function of an incubation at 6°C, for Δt hours (a: $\Delta t = 0$ h; b: $\Delta t = 243$ h; 1: $\Delta t = 26$ h; 2: $\Delta t = 51$ h; 3: $\Delta t = 74$ h; 4: $\Delta t = 97$ h; 5: $\Delta t = 121$ h; 6: $\Delta t = 164$ h; 7: $\Delta t = 196$ h; 8: $\Delta t = 236$ h). The heating rate was 0.5°C/min. Upon increasing Δt, the thermograms of the mixture exhibited two new growing endotherms at 22.5°C and 35.1°C.

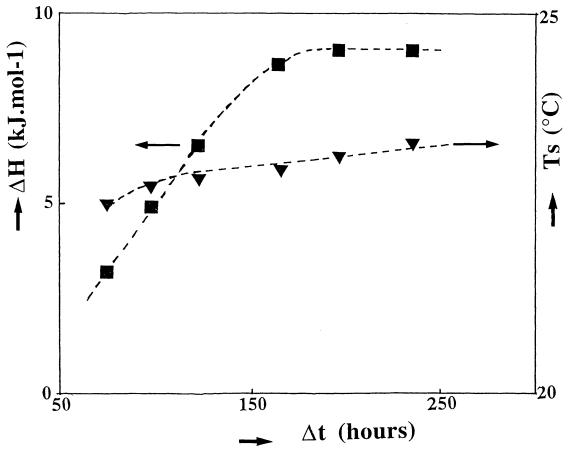

Fig. 10. Evolutions as a function of an incubation at 6°C, for Δt hours, of the enthalpy, ΔH, and the maximum temperature, Ts, of the endotherm appearing at the lowest temperature, in the thermograms of the mixture represented in Fig. 9.

22.1°C to 23.3°C and its enthalpy increased until a plateau of 9 kJ/mol (after $\sim$196 h for $R_A = 5\times10^{-3}$ and at a longer delay for $R_A = 2.5\times10^{-3}$, Fig. 10). Let us stress that the profile of the main endotherm in the mixture thermogram is not changed with respect to the thermogram of pure L-DPPC SUV, demonstrating the absence of perturbation of the packing of the L-DPPC bilayers by the presence of AmB.

3.4. AFM observations of ergosterol-containing mixtures II ($R_E = 5\times10^{-2}$ and 2×10^{-1}, $R_A = 2\times10^{-3}$), at room temperature

AFM images of the surface of ergosterol-containing AmB+L-DLPC mixtures II reveal two new facts with respect to those of the sterol-free AmB+L-DLPC mixtures II. First, most of the objects covering the surface of samples are hollow-centered (Fig. 11A,B). Second, these hollow objects could not be shifted by the tip even when the nominal applied force and the scanning rate were much higher than those of the imaging conditions.

The objects at the surface of the phospholipid sublayer, with and without ergosterol, were entirely dissolved by adding 10% v/v of DMF to the fluid cell: they were again identified as AmB aggregates. The size of these aggregates was polydispersed and the bigger the fewer. The presence of big AmB aggregates, despite the small initial proportion of AmB molecules in the mixtures II, deserves comments. In-

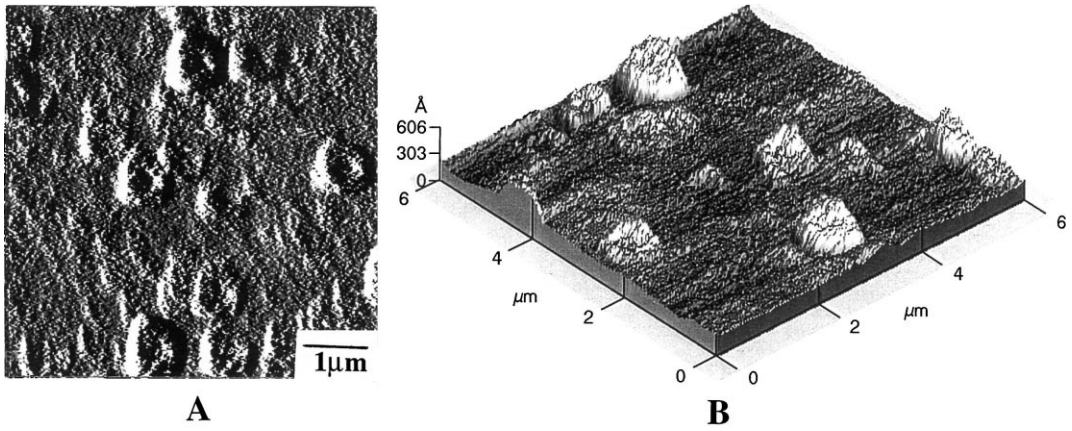

Fig. 11. Images of hollow-centered AmB aggregates on a mica-supported, ergosterol-containing mixture II (cf. Section 2, $R_E = 0.20$), obtained in contact mode in water. (A) 2D representation using the error signal [13]. This differential imaging mode gives an impression of relief but does not provide a height scale. (B) 3D representation of a topography image providing height and lateral dimensions of the hollow aggregates.

deed, what we observed, in fine, on the mica lens, was the result of the association of AmB with L-DLPC, occurring during the 14 h long incubation of the mixtures II above this mica lens (cf. Section 2). The initial composition of the mixture *before* any fixation on the mica and the stoichiometry of the association *after* this fixation, revealed by the AFM images, should not be confounded. Moreover, the *local* stoichiometric molar ratio AmB/L-DLPC, revealed by these images, can also be different from the *average* stoichiometric ratio determined in test tubes. Nevertheless, a rough calculation shows that these stoichiometries are not highly different. As a matter of fact, let us refer to Fig. 12 where five aggregates, with a mean volume of around 2×10^7 nm^3, are observed in a 50 µm^2 area. Knowing the AmB molecular volume (1 nm^3 [21]) and the surface density of L-DLPC molecules (3.6×10^6 µm^{-2}, from an area per L-DPPC polar head, in the fluid state, of 64 Å^2 [11]), a stoichiometric molar ratio L-DLPC/AmB = $1/R_A = 1.5$ results. This value is near to that previously obtained in test tubes for the first step of the binding ($1/R_A = 1$ [6]).

Complementary AFM observations were made in air, after elimination of water (intermittent contact mode imaging, cf. Section 2). The draining off of the interfacial water precluded any water-mediated H-bonds between AmB aggregates and the L-DLPC sublayer. Despite this fact, AmB aggregates remained visible. This second observation mode made it possible to sound more precisely the profiles of the hollow centers of AmB aggregates. As exemplified by Fig. 12 (height profiles B and C) these centers are V-shaped.

4. Discussion

Before discussing the above-described results, an outline of our knowledge about the architecture of AmB aggregates is necessary.

4.1. Architecture of aqueous AmB aggregates from calculations aimed at interpreting absorption and CD spectra

Our present knowledge about the architecture of AmB aggregates in water is based on simulations [21–23]. From such calculations, AmB aggregates are formed by self-association of quasi-planar dimers [21,23]. The stablest of these is obtained by joining side by side the polyene chains of two AmB molecules. However, the interpretation of the origin of the strong CD signal diverges in these different simulations. One study [23] attributes it to an intrinsic dimer asymmetry. Another study [21] attributes it to a helical array of the chromophores of stacked dimers (5.7 Å spaced) ('double helix model' [21], Fig. 1_3). From a theoretical viewpoint, there is nothing to prevent that such helices have an infinite length (J. Langlet, unpublished data). This latter model makes it possible to explain all the features of the absorption and CD spectra in the framework

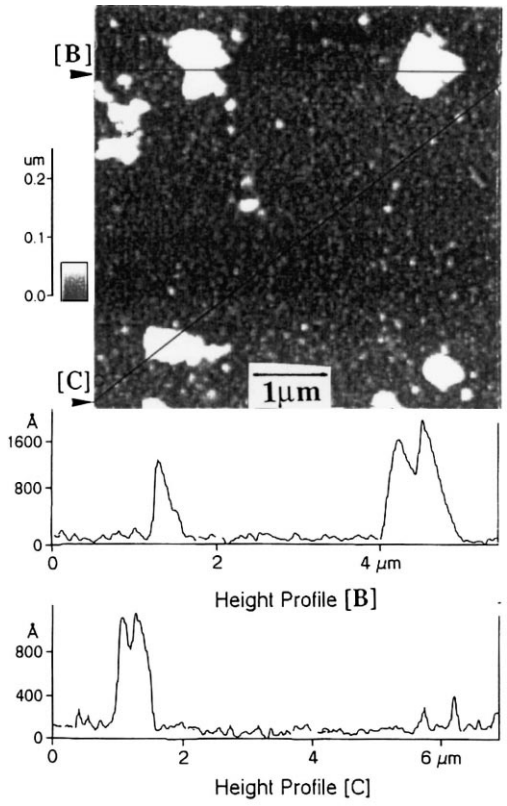

Fig. 12. Topography image of a mica-supported ergosterol-containing mixture II (cf. Section 2, $R_E = 5 \times 10^{-2}$), obtained in intermittent contact mode [12] in air, after a draining off of the water covering the preparation. In these conditions (no possibility of water-mediated H-bonds between AmB and L-DLPC molecules), only the sublayer-embedded AmB aggregates can remain fixed (cf. text). The presence of one non-hollow aggregate and hollow aggregates with cavities of different relative depths (height profiles B and C) suggests the occurrence of different stages of the digging of aggregates, subsequent to their embedding to the sublayer (cf. text). The gray bar is a representation of the differential heights.

of the exciton splitting theory. Let us recall that, in this theory, the geometric arrangement of two neighboring chromophores has a direct effect upon the allowedness of absorption and CD transitions [24]. If they are parallel (case A), the probability of the electronic transition to the short wavelength exciton level is much larger than that for the long wavelength level and the allowedness of both exciton transitions, in CD, is very small. In contrast, if the geometric arrangement of the two chromophores is oblique (case B), the two electronic and CD transitions are allowed; the two absorption bands overlap leading to a broad band and, in CD, a bisignate doublet, centered at the absorption maximum, appears [24]. In the double helix model of AmB aggregates, the blue shift of the absorption region with respect to that of monomers would result from the interaction between the two joined chromophores in each dimer (case A). On the other hand, the bisignate dichroic doublet would result from the rotation, in the stack, of the double chromophore of each dimer (case B).

Now, let us compare this model with our AFM observations. The smallest imaged AmB aggregates are viewed as 25 Å high slabs with lateral dimensions of around 130 nm (Fig. 4, height profile C). Knowing the diameter of the AmB ring (21 Å [25]), they could correspond to the gathering of a great number of the modeled helices, laid down on the surface. With regard to the biggest AmB aggregates, the high number of implicated AmB molecules ($\sim 10^5$) prevents any modeling at present. Nevertheless, let us signal that energetic considerations reveal the possibility of a polymorphism and a great diversity in size of AmB aggregates (J. Langlet, unpublished data).

4.2. Location of membrane-bound AmB aggregates when these membranes do not contain ergosterol

4.2.1. Mixtures II

AFM observations of sterol-free mixtures II, at room temperature, have shown that AmB aggregates remain at the surface of the L-DLPC sublayer.

4.2.2. Mixtures I

The stoichiometry of the binding of AmB aggregates to gel L-DPPC bilayers, determined at 6°C, $[1/R_A]_{final} = 17$, argues for a non-penetration of AmB aggregates into these bilayers. Indeed, in the gel phase, the lattice of phospholipid molecules is hexagonal and the replacement of the six nearest-neighboring molecules of one phospholipid molecule by 17 foreign molecules is hardly credible. Recently, calculations on absorption and CD spectra of AmB+L-DPPC SUV mixtures and AmBisome vesicles were made with the aim of determining the state of aggregation of AmB molecules in such preparations [26,27]. These calculations presupposed that AmB molecules were accommodated within the phospholipid bilayers. We do not agree with this viewpoint. Indeed, if AmB molecules were accommodated within the hydrophobic core of the bilayers (and a for-

tiori, in the form of micelles [27]), the organization of these bilayers would be perturbed and such a disorganization would be reflected on the DSC thermograms. Now, in our thermograms, the endotherm of the main transition (corresponding to the conformational change of fatty chains) appears as sharp as that of the AmB-free witness: no sign of perturbation of the hydrophobic core of the bilayers emerges.

The bonds binding AmB molecules to the L-DPPC bilayers are thought to be long-range, water-mediated, H-bonds, connecting the oxygen atoms of the phosphate groups of the L-DPPC polar heads and the hydroxyl groups of AmB molecules, at the bilayer–water interface. In Fig. 1_3 is schematized how the mutual arrangement of the AmB and phospholipid polymolecular assemblies at this interface could be envisioned.

4.3. Transformations resulting from the binding between AmB and L-DPPC molecules at the bilayer–water interface

4.3.1. L-DPPC-induced inversion of the chirality of AmB aggregates

The occurrence of an isodichroic point on the CD spectra, registered during the binding of AmB aggregates to L-DPPC bilayers (Figs. 5B and 6), means that these aggregates are transformed from one conformation into another. Referring to the double helix model of these aggregates [21], the inversion of the sign of the dichroic doublet means that this transformation is a reversal of the helicity sign. Now, L-DPPC molecules are also chiral ($\Delta\varepsilon = +0.1$ M^{-1} cm^{-1}, at 220 nm, not shown). Moreover, as recently demonstrated [28,29], this chirality leads to a chiral arrangement of L-DPPC molecules in monolayers and bilayers, when they are in the gel state. Consequently, the orientation of the L-DPPC polar heads, known as being almost parallel to the surface of the membranes [30], is ordered in conformity with the chirality of the implied DPPC enantiomer. The P^--N^+ dipoles of L-DPPC turn clockwise at the interface with water (Fig. 1_3). On the other hand, in helical AmB aggregates, envisioned as laid down on this interface, the polyene chains turn counterclockwise, as implied by the sign of the dichroic doublet (long wavelength negative, short wavelength positive). Their binding to gel L-DPPC bilayers leads to a reversal of their helicity. As visualized by the sketch of Fig. 1_3, we think that the AmB molecules, bound to L-DPPC molecules at the interface, can be dragged along by the clockwise rotation of the P^--N^+ dipoles of the L-DPPC polar heads. Due to steric crowding such a transformation could be thought difficult. However, it would be facilitated if the helical aggregates are previously stretched. Two facts argue for such a stretching. First, as noted in Fig. 1_3, AmB dimers are spaced by 5.7 Å (double helix model [21]) while L-DPPC molecules are spaced by 7.8 Å [11], at the interface: their mutual binding could induce an increase of the distance between AmB dimers. Second, the lowering of the dichroic signal indicates a decrease of the excitonic coupling between the chromophores of neighboring dimers, again arguing for an increase of their distance. Reinforcing this interpretation, no reversal of the dichroic doublet occurs when the L-DPPC bilayers are in the fluid state (no ordered orientation of the L-DPPC polar heads).

Similar transfers of chiral information have been reported in recent studies [31–35]. These studies have especially shown how helical structures (like that of AmB aggregates) can be influenced by substituents bearing a chiral center (like L-DPPC molecules) [31]. They testify to the feasibility of such transfers even through loose H-bonds [33,34]. Moreover, they demonstrate that the chiral distortion forces are able to put in motion a number of molecules as large as that contained in polymer chains or in the AmB aggregates [32,35]. Finally, let us recall that we have reported a similar inversion of the sign of the AmB dichroic doublet during the binding of AmB to L-DLPC bilayers [6].

4.3.2. AmB-induced transformation of L-DPPC bilayers

The thermograms of the AmB+L-DPPC mixtures exhibit, for increasing incubation times at 6°C, two growing endotherms at 35°C and around 23°C (Figs. 9 and 10). The characteristics of the latter (temperature and irreversibility) make it possible to assign it to the subtransition of the L-DPPC bilayers [36]. But for pure L-DPPC, an incubation, even prolonged, at 6°C does not trigger such a transition [37], as confirmed by its absence on the thermograms of our witness (Fig. 9, traces a and b). Such a transforma-

tion can be related, as demonstrated by Kodama et al. [36], to a modification of the thermodynamic state of the L-DPPC-bound water molecules, at the interface. The occurrence of a possible action of AmB on this interfacial water is in progress by Fourier transform infrared investigations.

Let us note that, in a previous calorimetric investigation of DPPC+AmB mixtures, with AmB concentrations higher by a factor of 10 than ours [38], the endotherm corresponding to the main transition exhibited a shoulder on its high-temperature side. A decomposition of this endotherm caused two components to appear which were attributed to structures within the bilayers which would be responsible for the permeabilizing action of AmB. We are sceptical about this interpretation. As a matter of fact, a similar shoulder was already observed on the thermograms of mixtures of DPPC+nystatin (another polyene antibiotic) [39]. However, despite the appearance of this shoulder, nystatin aggregates remained at the interface with water of PC bilayers [6].

4.4. Membrane-embedding and subsequent digging of AmB aggregates when the membranes contain ergosterol

AFM images of ergosterol-containing mixtures II, compared with those of sterol-free mixtures II, reveal the two following facts: (i) AmB aggregates persist in the absence of the interfacial water (Fig. 12); (ii) they become not displaceable by the tip. These facts imply that AmB aggregates are embedded in the L-DLPC sublayer. This fact crosschecks results of monolayer experiments. Such experiments have proved that, when phospholipid monolayers contain ergosterol, AmB molecules are accommodated within them [40–43]. They have especially shown that a compression of a mixed AmB/egg phosphatidylcholine monolayer, up to 20 mN m^{-1} (close to the equilibrium lateral pressure in the lamellar bilayers) leads to a desorption of AmB molecules, except if this monolayer contains ergosterol [40].

Subsequent to their embedding, AmB aggregates become hollow-centered (Figs. 11 and 12). The understanding of this phenomenon requires a novel examination of the architecture of AmB aggregates in water. In the sketch of one AmB dimer in Fig. 1_2, the hydrophilic parts of AmB molecules are external and the hydrophobic parts internal: it is incompatible with an embedding in the hydrophobic core of a phospholipid bilayer. However, as sketched in Fig. 1_2, such an embedding can be made if the polyene chains are transferred to the periphery. Now, let us consider a stack of dimers laid down, perpendicularly to the interface. The transfer to the periphery of the polyene chains of the dimer at the basis of this stack generates a gap and can lead to a cascade of similar transfers in the dimers above it resulting in a central caving. However, to maintain this stack in such a position an adhesion force is required. In the absence of any osmotic stress of the bilayer, ensuring this adhesion [4], we think that the presence of membranous ergosterol facing the stack is responsible for its fixation. Indeed, the idea of such a turning inside out of AmB aggregates has already been proposed [44], but, then, it did not have the support of the direct observation of a central digging of AmB aggregates.

Pursuing this interpretation, the sublayer-embedded AmB aggregates in course of digging naturally appear to us as precursors of AmB pores, the aperture of which would be invisible. We think that the V-shaped hollow centers of the AmB aggregates have a terminal aperture but it has escaped our observations because of the bulkiness of the extremity of our tip (a half-sphere 60 nm in diameter). Indeed, the generally postulated size of the aperture of AmB pores is 7–10 Å in diameter [45]. There is nothing to prevent that this small aperture could be the invisible terminal aperture of the sublayer-embedded hollow-centered AmB aggregates.

5. Conclusion

Our results have revealed three original undeniable facts. First, in the absence of ergosterol, two remarkable phenomena, occurring during the binding of AmB aggregates to L-DPPC bilayers, have been disclosed. On the one hand, a L-DPPC-induced inversion of the helicity of AmB aggregates has been evidenced. On the other hand, a AmB-induced gel-to-subgel transformation of the L-DPPC bilayers has been established. Such transformations are thought to be due to interactions between AmB and phospholipid polymolecular assemblies at the bilayer–water interface.

Second, in the presence of ergosterol, AFM images have directly demonstrated that the main role of ergosterol is to enable the embedding of AmB aggregates in phospholipid bilayers. In addition, the central digging of these aggregates, subsequent to their embedding, has given us a clue to understand one mechanism of the formation of AmB pores. We think, indeed, that this digging represents the visible aspect, at a large scale, of a process occurring at a much smaller scale, namely the building of an AmB pore.

Acknowledgements

The first author is indebted to Dr. J. Bolard for his encouragement.

References

[1] S. Hartsel, J. Bolard, Amphotericin B: new life for an old drug, Trends Pharmacol. Sci. 17 (1996) 445–449.
[2] B.E. Cohen, Amphotericin B toxicity and lethality: a tale of two channels, Int. J. Pharm. 162 (1998) 95–106.
[3] R.A. Brutyan, P.J. McPhie, On the one-sided action of amphotericin B on lipid bilayer membranes, J. Gen. Physiol. 107 (1996) 69–78.
[4] T. Ruckwart, A. Scott, J. Scott, P. Mikulecky, S.C. Hartsel, Lipid stress dependence of amphotericin B ion selective channels in sterol-free membranes, Biochim. Biophys. Acta 1372 (1998) 283–288.
[5] B.V. Cotero, S. Rebolledo-Antunez, I. Ortega-Blake, On the role of sterol in the formation of the amphotericin B channel, Biochim. Biophys. Acta 1375 (1998) 43–51.
[6] J. Milhaud, B. Michels, Binding of nystatin and amphotericin B with sterol-free L-dilauroylphosphatidylcholine bilayers resulting in the formation of dichroic lipid superstructures, Chem. Phys. Lipids 101 (1999) 223–235.
[7] J.C. Stewart, Colorimetric determination of phospholipids with ammonium ferrothiocyanate, Anal. Biochem. 104 (1980) 10–14.
[8] P.L. Privalov, Scanning microcalorimeters for studying macromolecules, Pure Appl. Chem. 52 (1980) 479–497.
[9] E. Kalb, S. Frey, L.V. Tamm, Formation of supported planar bilayers by fusion of vesicles to supported phospholipid monolayers, Biochim. Biophys. Acta 1103 (1992) 307–316.
[10] P. Nollert, H. Kiefer, F. Jähnig, Lipid vesicle adsorption versus formation of planar bilayers on solid surfaces, Biophys. J. 69 (1995) 1447–1455.
[11] J.F. Nagle, S. Tristram-Nagle, Structure of lipid bilayers, Biochim. Biophys. Acta 1469 (2000) 159–195.
[12] Y.F. Dufrêne, G.U. Lee, Advances in the characterization of supported lipid films with AFM, Biochim. Biophys. Acta 1509 (2000) 14–41.
[13] C.A.J. Putman, K.O. Van der Werf, B.G. De Grooth, N.F. Van Hulst, J. Greve, P.K. Hansma, A new imaging mode in AFM based on the error signal, SPIE 1639 (1992) 198–204.
[14] J. Rädler, M. Radmacher, H.E. Gaub, Velocity-dependent forces in atomic force microscopy imaging of lipid films, Langmuir 10 (1994) 3111–3115.
[15] J. Bolard, M. Seigneuret, G. Boudet, Interaction between phospholipid bilayer membranes and the polyene antibiotic amphotericin B. Lipid state and cholesterol content dependence, Biochim. Biophys. Acta 599 (1980) 280–293.
[16] C.R. Cantor, P.R. Schimmel, Biological Structure and Function, Part II, W.H. Freeman and Company, San Francisco, CA, 1984, pp. 390–406.
[17] M. Caffrey, G.W. Feigenson, Fluorescence quenching in model membranes 3. Relationship between calciumadenotriphosphatase enzyme activity and the affinity of the protein for phosphatidylcholines with different acyl chain characteristics, Biochemistry 20 (1981) 1949–1961.
[18] N.M. Witzke, R. Bittman, Dissociation kinetics and equilibrium binding properties of polyene antibiotic complexes with phosphatidylcholine/sterol vesicles, Biochemistry 23 (1984) 1668–1674.
[19] K.A. Connors, Binding Constants. The Measurement of Molecular Complex Stability, Wiley Interscience, New York, 1987, chapter 2.
[20] R.L. Biltonen, D. Lichtenberg, The use of DSC as a tool to characterize liposome preparations, Chem. Phys. Lipids 64 (1993) 129–142.
[21] P. Millié, J. Langlet, J. Bergés, J. Caillet, J.P. Demaret, Self-association of amphotericin B in water. Theoretical energy and spectroscopy studies, J. Phys. Chem. B. 103 (1999) 10883–10891.
[22] J. Caillet, J. Bergés, J. Langlet, Theoretical study of the self-association of amphotericin B, Biochim. Biophys. Acta 1240 (1995) 195.
[23] J. Mazerski, E. Borowski, Molecular dynamics of amphotericin B. II. Dimer in water, Biophys. Chem. 57 (1996) 205–217.
[24] R.V. Person, B.R. Peterson, D.A. Lightner, Bilirubin conformational analysis and circular dichroism, J. Am. Chem. Soc. 116 (1994) 42–59.
[25] P. Ganis, G. Avitabile, W. Mechlinski, C.P. Schaffner, Polyene macrolide antibiotic amphotericin B. Crystal structure of the N-iodoacetyl derivative, J. Am. Chem. Soc. 93 (1971) 4560–4564.
[26] M. Gagos, R. Koper, W.I. Gruszecki, Spectrophotometric analysis of organisation of dipalmitoylphosphatidylcholine bilayers containing the polyene antibiotic amphotericin B, Biochim. Biophys. Acta 1511 (2001) 90–98.
[27] G. Fujii, J.E. Chang, T. Coley, B. Steere, The formation of amphotericin B ion channels in lipid bilayers, Biochemistry 36 (1997) 4959–4968.
[28] X.M. Yang, D. Xiao, S.J. Xiao, Z.H. Lu, Y. Wei, Observa-

tion of chiral domain morphology in a phospholipid Langmuir-Blodgett monolayer by AFM, Phys. Lett. A 193 (1994) 195–198.
[29] P. Walde, E. Blöchliger, Circular dichroic properties of phosphatidylcholine liposomes, Langmuir 13 (1997) 1668–1671.
[30] H. Hauser, I. Pascher, S. Sundell, Preferred conformation of the diacylglycerol moiety of phospholipids, in: R. Brasseur (Ed.), Molecular Description of Biological Membranes by Computer-aided Conformational Analysis, Vol. I, Part 1B, CRC Press, Boca Raton, FL, 1990, chapter 1.
[31] T. Mizutani, S. Yagi, T. Morinaga, T. Nomura, S. Takagishi, S. Kitagawa, H. Ogoshi, Helical chirality induction by point chirality at helix terminal, J. Am. Chem. Soc. 121 (1999) 754–759.
[32] E. Yashima, K. Maeda, Y. Okamoto, Memory of macromolecular helicity assisted by interaction with achiral small molecules, Nature 399 (1999) 449–451.
[33] L.J. Prins, J. Huskens, F. De Jong, P. Timmerman, D.N. Reinhoudt, Complete asymmetric induction of supramolecular chirality in a hydrogen-bonded assembly, Nature 398 (1999) 498–502.
[34] K. Konishi, K. Yahara, H. Toshishige, T. Aida, S. Inoue, A novel anion-binding chiral receptor based on a metalloporphyrin with molecular assymetry. Highly enantioselective recognition of amino acid derivatives, J. Am. Chem. Soc. 116 (1994) 1337–1344.
[35] R. Oda, I. Hue, M. Schmutz, S.J. Candau, Tuning bilayer twist using chiral counterions, Nature 399 (1999) 566–569.
[36] M. Kodama, H. Hashigami, S. Seki, Role of water molecules in the subtransition of the L-DPPC-water system, J. Colloid Interface Sci. 117 (1987) 497–504.
[37] S. Tristram-Nagle, M.C. Wiener, C.P. Yan, J.F. Nagle, Kinetics of the subtransition in DPPC, Biochemistry 26 (1987) 4288–4294.
[38] I. Fournier, J. Barwicz, P. Tancréde, The structuring effects of amphotericin B on pure and ergosterol or cholesterol-containing dipalmitoylphosphatidylcholine bilayers: a differential scanning calorimetry study, Biochim. Biophys. Acta 1373 (1998) 76–86.
[39] J. Bolard, J. Milhaud, Interaction of the anti-candida amphotericin B (and other polyene antibiotics) with lipids, in: R. Prasad, M.A. Ghannoum (Eds.), Lipids of Pathogenic Fungi, CRC Press, Boca Raton, FL, 1996, chapter 12.
[40] M. Saint-Pierre Chazalet, C. Thomas, M. Dupeyrat, C.M. Gary-Bobo, Amphotericin B-sterol complex formation with egg phosphatidylcholine: a monolayer study, Biochim. Biophys. Acta 944 (1988) 477–486.
[41] J. Barwicz, P. Tancréde, The effect of aggregation state of amphotericin B on its interactions with cholesterol or ergosterol-containing phosphatidylcholine monolayers, Chem. Phys. Lipids 85 (1997) 145–155.
[42] J.C. Garrigues, I. Rico-Lattes, E. Perez, A. Lattes, Comparative study for the incorporation of a new antifugal family of neoglycolipids and amphotericin B in monolayers containing phospholipids and cholesterol or ergosterol, Langmuir 14 (1998) 5968–5971.
[43] R. Seoane, J. Minones, O. Conde, M. Casas, E. Iribarnegaray, Molecular organisation of amphotericin B at the air-water interface in the presence of sterols: a monolayer study, Biochim. Biophys. Acta 1375 (1998) 73–83.
[44] J. Bolard, P. Legrand, F. Heitz, B. Cybulska, One-sided action of amphotericin B on cholesterol-containing membranes is determined by its self-association in the medium, Biochemistry 30 (1991) 5707–5715.
[45] M. Baginski, H. Resat, J.A. McCammon, Molecular properties of amphotericin B membrane channel: a molecular dynamics simulation, Mol. Pharmacol. 52 (1997) 560–570.